The Astrophysical Journal Supplement Series, 267:45 (8pp), 2023 August https://doi.org/10.3847/1538-4365/ace59a

Three-day Forecasting of Solar Wind Speed Using SDO/AIA Extreme-ultraviolet Images by a Deep-learning Model

Jihyeon Son[1], Suk-Kyung Sung[2], Yong-Jae Moon[1,2], Harim Lee[2], and Hyun-Jin Jeong[2]
[1] School of Space Research, Kyung Hee University, Yongin, 17104, Republic of Korea; moonyj@khu.ac.kr
[2] Department of Astronomy and Space Science, Kyung Hee University, Yongin, 17104, Republic of Korea
Received 2023 March 23; revised 2023 June 15; accepted 2023 July 6; published 2023 August 10

Abstract

In this study, we forecast solar wind speed for the next 3 days with a 6 hr cadence using a deep-learning model. For this we use Solar Dynamics Observatory/Atmospheric Imaging Assembly 211 and 193 Å images together with solar wind speeds for the last 5 days as input data. The total period of the data is from 2010 May to 2020 December. We divide them into a training set (January–August), validation set (September), and test set (October–December), to consider the solar cycle effect. The deep-learning model consists of two networks: a convolutional layer–based network for images and a dense layer–based network for solar wind speeds. Our main results are as follows. First, our model successfully predicts the solar wind speed for the next 3 days. The rms error (RMSE) of our model is from 37.4 km s^{-1} (for the 6 hr prediction) to 68.2 km s^{-1} (for the 72 hr prediction), and the correlation coefficient is from 0.92 to 0.67. These results are much better than those of previous studies. Second, the model can predict sudden increase of solar wind speeds caused by large equatorial coronal holes. Third, solar wind speeds predicted by our model are more consistent with observations than those by the Wang–Sheely–Arge–ENLIL model, especially in high-speed-stream regions. It is also noted that our model cannot predict solar wind speed enhancement by coronal mass ejections. Our study demonstrates the effectiveness of deep learning for solar wind speed prediction, with potential applications in space weather forecasting.

Unified Astronomy Thesaurus concepts: The Sun (1693); Convolutional neural networks (1938); Solar wind (1534)

1. Introduction

The study of space weather has become increasingly important nowadays because of its significant effects not only on satellites in space but also to humans on Earth. One of the key components determining the condition of space weather is the solar wind, which is an outward flow of charged particles released from the Sun. Typically, the solar wind can be classified into two types by speed: slow solar wind ($v \leqslant 400$ km s^{-1}) and fast solar wind ($v \geqslant 650$ km s^{-1}) (Bravo & Stewart 1997). The interaction between the fast solar wind and the ambient slow solar wind produces a region known as the corotating interaction region (CIR). CIR is well known to be one of drivers of interplanetary shocks. At the leading edge and the trailing edge of the CIR, forward shocks and reverse shocks are formed, respectively (Gosling & Pizzo 1999; Pitňa et al. 2021). The solar wind streams with high pressure in the CIR mainly contribute to the geomagnetic activity via magnetic reconnection with the magnetosphere of the Earth (Richardson et al. 2000; Tsurutani et al. 2006).

Coronal holes, which are an open magnetic field region, are the source of high-speed solar wind (Nolte et al. 1976; Zirker 1977; Hassler et al. 1999), and it is known that there is a relationship between coronal holes, CIRs, and geomagnetic disturbances (Vršnak et al. 2007a, 2007b; Choi et al. 2009). de Toma (2011) investigated the evolution of the coronal holes and their implications for high-speed solar wind between 2006 and 2009, and found that large and low-latitude coronal holes are important sources of recurrent high-speed solar wind streams. Therefore, it is essential to forecast the solar wind speed by investigating the relationship between solar phenomena and solar wind.

There have been a lot of models to predict the solar wind speed using various methods such as physics-based models (Odstrcil 2003; Reiss et al. 2020; Elliott et al. 2022), empirical models (Owens et al. 2013; Bussy-Virat & Ridley 2014; Rotter et al. 2015), and artificial intelligence–based models (Poggi et al. 2003; Liu et al. 2011; Yang et al. 2018). The Wang–Sheely–Arge (WSA) model (Wang & Sheeley 1990, 1992; Arge & Pizzo 2000) can predict the background solar wind speed at the outer boundary of the coronal magnetic field, employing a potential field source surface model (Schatten et al. 1969; Altschuler & Newkirk 1969) and the Schatten current sheet model (Schatten 1971) of the steady-state corona. The WSA model is coupled with the ENLIL model (Odstrcil 2003), which enables simulations of solar wind disturbances using MHD approximations from the solar corona up to 1 au and beyond in the inner heliosphere. The WSA-ENLIL model has been operated in the Space Weather Prediction Center of the National Oceanic and Atmospheric Administration.

Recently, deep learning has been applied to various fields of space weather, including solar wind speed prediction. For example, Upendran et al. (2020) predicted solar wind speed of the next day using extreme ultraviolet (EUV) images and visualized how the model used data to make predictions. Sun et al. (2021) proposed a model based on the two-dimensional attention mechanism for forecasting the solar wind speed 24 hr ahead. Raju & Das (2021) used a convolutional neural network–based model for daily solar wind speed prediction, introducing an adaptive time-delay method.

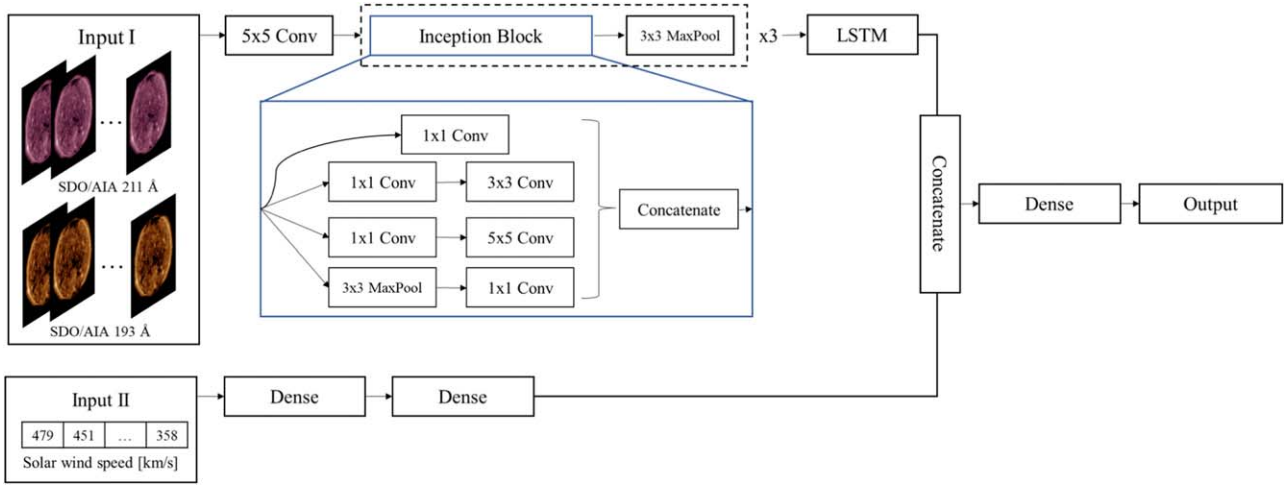

Figure 1. Architecture of our deep-learning model. It consists of two input layers, to which the solar images (Input I) and solar wind speed data (Input II) are respectively entered. The images pass several convolution networks and one LSTM layer, and the solar wind speed data flow into two dense layers. They are concatenated and pass one dense layer at the end of the network, and then the targets (sequential solar wind speed values) are predicted.

In this study, we propose a deep-learning model to predict the solar wind speed at Earth for the next 3 days with a 6 hr cadence. In contrast to previous studies that make predictions of solar wind speeds at a single time point, our model has the capability to sequentially predict them with a higher time resolution. We use solar EUV images, which can provide the characteristics of solar coronal holes, and solar wind speeds themselves as input data. The deep-learning model consists of two networks, including a convolutional layer–based network for images and a dense layer–based network for solar wind speeds. This paper is organized as follows. In Section 2 and Section 3, the data and method used in this study are described, respectively. In Section 4, we show the results of our model and discuss them. Finally, in Section 5, we summarize this study.

2. Data

For this work, we obtain the hourly averaged solar wind speed data from OMNIWeb[3] of the Space Physics Data Facility (King & Papitashvili 2005). And we use solar EUV images observed in 211 and 193 Å from the Solar Dynamics Observatory (SDO; Pesnell et al. 2012)/Atmospheric Imaging Assembly (AIA; Lemen et al. 2012) indicating the characteristics of coronal holes. We make 6 hr averaged solar wind speed data and select the EUV images observed at the closest time of each solar wind speed data (00, 06, 12, and 18 UT). We use the data from 2010 May to 2020 December (total 15,203 data pairs), excluding cases where there is no observation or poor image quality (quality $\neq 0$ in fits header). All EUV images are preprocessed by rotating, centering, exposure compensation, and degradation compensation using the SolarSoft library. Then the images are resized to 64×64 from the original size ($4k \times 4k$) to optimize memory usage and converted into PNG files. We use 64×64 size images because we think that it would not be very necessary for the deep-learning model to capture all the complex shapes of coronal holes. Only their location and size information would be enough for solar wind prediction task. In fact, we have tried to train the model with images of 128×128 size; the performance of the model is almost same.

The input data of the previous 5 days from the prediction time are used as input data of the model by considering the traveling time of solar winds from the Sun to the Earth. It is determined by several trials changing the input length from 3 to 6 days. The solar wind speed data are entered with a 6 hr cadence, and solar images are done with a 12 hr cadence. Target data are the 3 day ahead solar wind speed with a 6 hr cadence. The total period of the data is from 2010 May to 2020 December, which covers one solar cycle. Considering the solar cycle effect, we divide the data set as follows: all January–August data are used for the training set (9992), all September data for the validation set (1321), and all October–December data for the test set (3890). We check each probability distribution of the training and test sets. It seems that the training data and test data have almost the same distributions, and we can say that there are few biases in our data set. And we carefully determined the periods of the training and test data sets. If the training and test sets are randomly divided, the dates of the training data and the test data may overlap too much. In that case, the input data are almost the same for both data sets so that the model results would be quite successful. Therefore, we think the way we divide the data set is the most appropriate to train the model. The data set we used in this study covers only solar cycle 24, which is a rather weak cycle, and our model may be biased toward the tendency of this period. When our model is applied in solar cycle 25, some additional training data may be used to improve the model.

3. Method

Since we use both the solar images and solar wind speed values as input data, we need two networks to handle different types of data. Figure 1 shows the architecture of our deep-learning model. For the network of the image data, we use the Inception block in GoogLenet (Szegedy et al. 2014) for our model. The Inception block was used and its performance was verified by Upendran et al. (2020) for the solar wind speed prediction task. The key advantage of the Inception block is using 1×1 convolutional layers. With this, the amount of computation can be reduced effectively. As a result,

[3] https://omniweb.gsfc.nasa.gov/

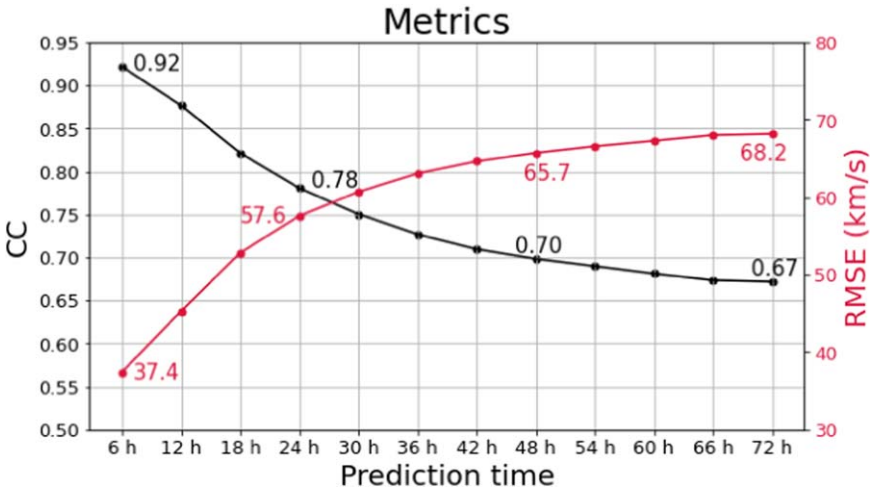

Figure 2. CC and RMSE of our model for given prediction times. The left axis is CC (black) and the right axis is RMSE (red).

convolutional layers can be stacked deeper with fewer memories. In addition, the model can extract visual information in multiscale because different kernel sizes are used in parallel on the same input. The structure of the Inception block is shown in the blue box of Figure 1. The solar images pass through one three-dimensional convolutional layer followed by three Inception blocks, and one long short-term memory (LSTM; Hochreiter & Schmidhuber 1997). LSTM is a well-known layer to be effective for sequential data. The other network for solar wind speed data consists of two dense layers. At the end, the two networks are concatenated, and pass one dense layer, and then the model finally predicts the sequential solar wind speeds. Every convolutional layer is followed by a max pooling layer. Rectified linear unit (Nair & Hinton 2010) activation is used at the convolutional layers and LSTM layer, and scaled exponential linear unit (Klambauer et al. 2017) activation is used at the dense layers. We use mean square error (MSE) as a loss function for training, and an Adam optimizer (Kingma & Ba 2014) with a learning rate of 0.0001 to optimize the model.

4. Results and Discussion

We evaluate the performance of our model in view of the correlation coefficient (CC) and rms error (RMSE) between real values and predicted values by our model for given prediction times: 6, 12, 18, 24, ..., 72 hr. The CC and RMSE are given by

$$\mathrm{CC} = \frac{\sum_{i=1}^{N}(X_i - \bar{X})(Y_i - \bar{Y})}{\sqrt{\sum_{i=1}^{N}(X_i - \bar{X})^2}\sqrt{\sum_{i=1}^{N}(Y_i - \bar{Y})^2}}, \quad (1)$$

$$\mathrm{RMSE} = \sqrt{\frac{\sum_{i=1}^{N}(X_i - Y_i)^2}{N}}, \quad (2)$$

respectively. X_i, Y_i, $\bar{X}$, $\bar{Y}$, and N denote ith predicted values, ith real values, their average values, and the total number of data, respectively. The RMSE shows overall differences between the observation values and the predicted values by the model, and the CC shows how well the model captures the pattern of the solar wind speeds. The lower the RMSE and the closer CC is to 1, the better the performance. As shown in Figure 2, the CC of our model is from 0.92 (for the 6 hr prediction) to 0.67 (for the 72 hr prediction), and the RMSE is from 37.4 to 68.2 km s^{-1}. Table 1 shows comparison of the results of the 24 hr prediction by our model with those of other solar wind prediction models. Even though they cannot be compared directly to the results due to the difference of target time resolution and length, we can say that our model successfully predicts solar wind speeds in view of the metrics.

Table 1
Comparison of the Results between Our Model and Other Models

Model	RMSE	CC	Prediction Time (hr)
Upendran et al. (2020)	76.4	0.55	24 (1 day average)
Raju & Das (2021)	76.3	0.57	24 (1 day average)
Sun et al. (2021)	62.8	0.79	24 (1 hr average)
Our model	57.6	0.78	24 (6 hr average)

Figure 3 shows the RMSE and CC of our model for each year (2011–2020). During the solar maximum phase (2013–2014), the performance is not so good compared to other years, probably because of many coronal mass ejections (CMEs). After the maximum phase since 2015, the CCs are greater than 0.85 and RMSEs in speed are smaller than 70 km s^{-1}, demonstrating that our prediction is quite successful.

Figure 4 shows good examples of the results of our model when the solar wind speeds increase, and Figure 5 shows when they decrease. These examples show that our model can predict both increase and decrease of solar wind speeds. Especially, our model successfully predicts not only the values, but also the timing of the rising of solar wind speeds. We can find the reason for the good prediction shown in Figure 4 from the input data, i.e., solar EUV images. Figures 6(a) and (b) shows the input images (193 and 211 Å images) of events in Figures 4(a) and (b), respectively. These two examples have in common that there are noticeable equatorial coronal holes appearing from the east limb and moving to the west limb. This fact implies that the model should successfully learn that the sources of fast solar winds are coronal holes (Nolte et al. 1976; Zirker 1977; Hassler et al. 1999).

We compare solar wind speeds predicted by our model with those by the WSA-ENLIL model. The WSA-ENLIL model produces simulation results of the solar wind using a radial magnetic field from a synoptic magnetogram and with coronal

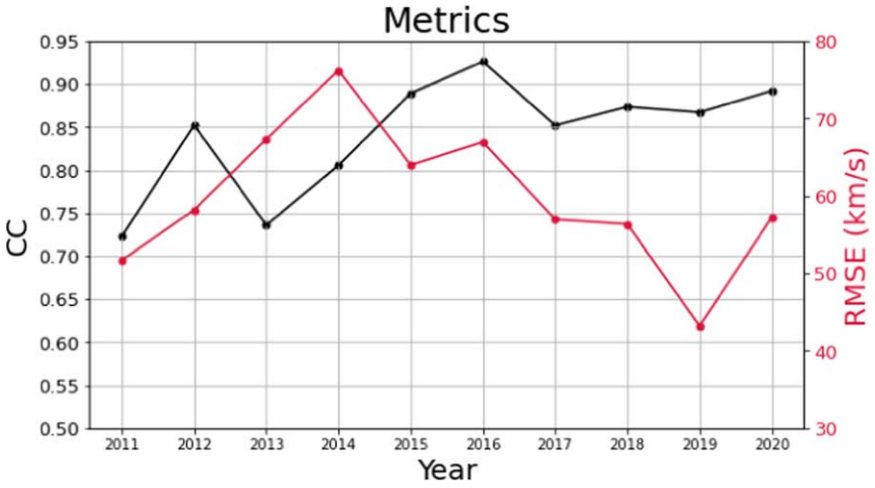

Figure 3. CC and RMSE of our model for each year (2011–2020). The left axis is CC (black) and the right axis is RMSE (red).

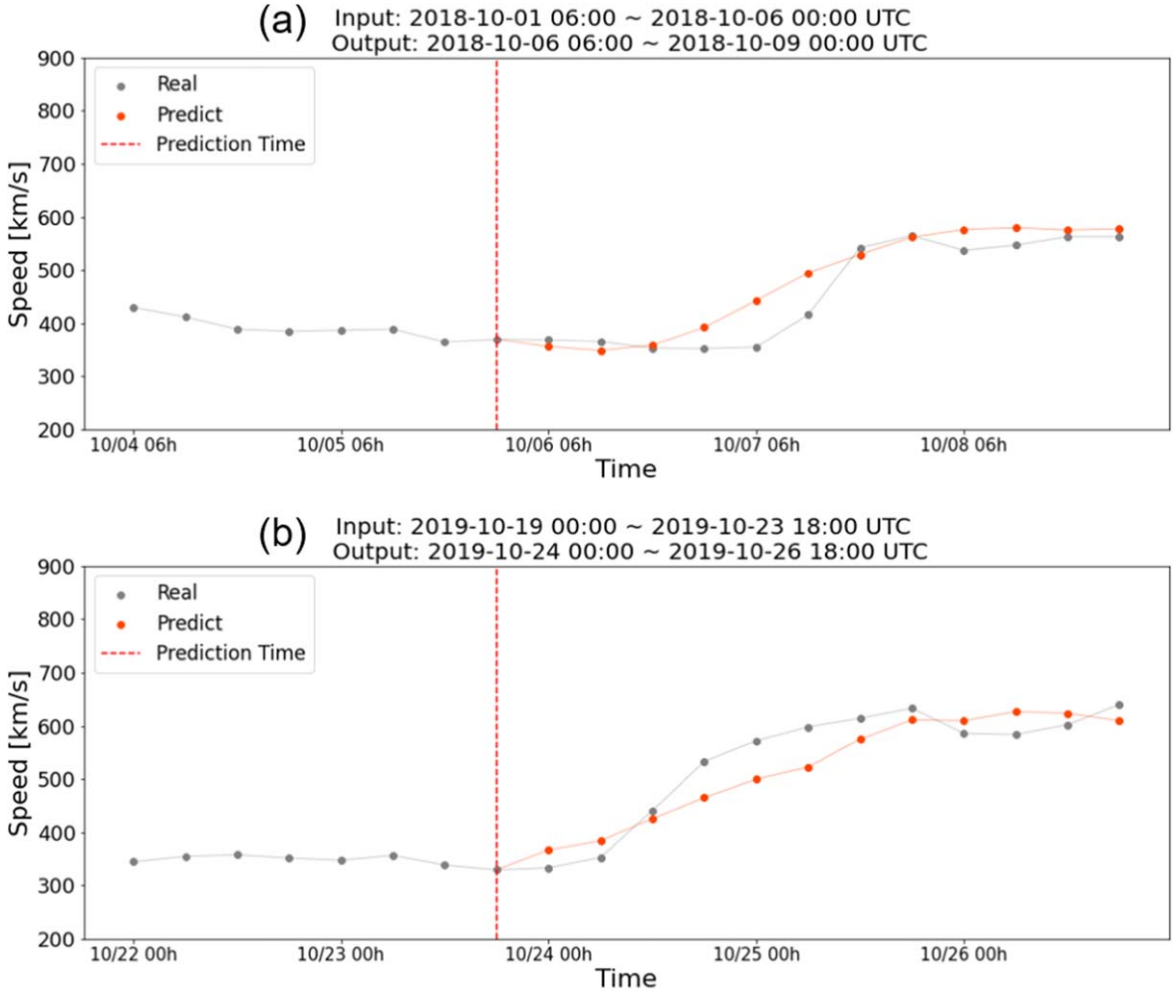

Figure 4. Two good examples of results from our model when there is the enhancement of solar wind speeds caused by coronal holes. The gray line means observation data, and the orange one means prediction values by our model. The red dashed line is a forecast starting time.

base plasma temperature and density as input data. Figure 7 shows the results during Carrington rotation (CR) 2209, which includes the period in Figure 4(a). Since we compare solar wind speeds at 1 au where it takes 3–4 days for the solar wind to arrive at the Earth, we show a series of 72 hr predictions with a 6 hr cadence by our model during the same period. Here the result of the WSA-ENLIL model is obtained from CORHEL-MAS_WSA_ENLIL by requesting it from the Community Coordinated Modeling Center (CCMC) at the Goddard Space Flight Center (GSFC). For this we use GONG data for input magnetic fields and all other optional parameters are default values. For comparison the one-run result of the WSA-ENLIL

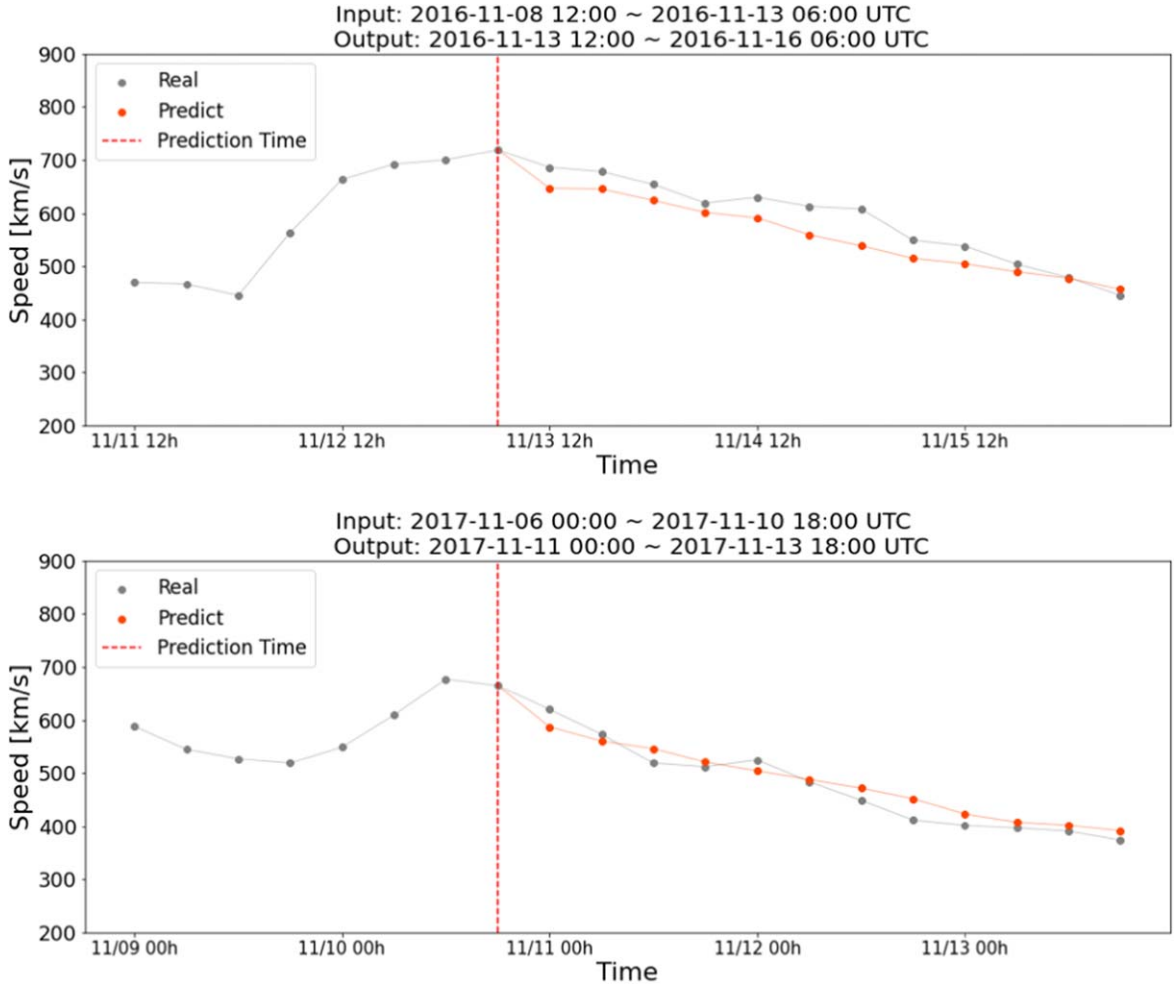

Figure 5. Two good examples of results from our model when the solar wind speeds decrease. The gray line shows observation data, and the orange one shows prediction values by our model. The red dashed line is a forecast starting time.

model is given for the CR 2209, starting from 2018 September 29. It is noted that the results of the WSA-ENLIL model can be significantly improved by changing the input synoptic maps and parameters (Sachdeva et al. 2019; Odstrcil et al. 2020). In Figure 7, two regions of fast solar winds faster than 600 km s^{-1} are shown in this period. At least we can say that our model can predict well both fast solar wind streams with high accuracy, when compared to the WSA-ENLIL model. More detailed comparisons should be given in the future. In addition, Owens et al. (2008) calculated performance of the WSA-ENLIL model with a 1 hr cadence over an 8 yr period (1995–2001) at L1 point. Their RMSE is 97.2 km s^{-1} during that period, and the RMSE of our model for 72 hr prediction results is 68.2 km s^{-1} during our test period (every October–December in 2010–2020). We may say that our model is comparable to or even better than the WSA-ENLIL model in view of near-Earth solar wind speed prediction.

During the period of the test data, we identify a total of 36 high-speed streams according to the criteria by Jian et al. (2015). Our model can capture the increase of solar wind speed for 25 of these events (about 70%). There are 12 interplanetary CMEs (ICMEs) resulting in increasing solar wind speeds, and our model cannot predict all of them. Figure 8 shows an example of poor prediction of our model. The model cannot catch the sudden increase of solar wind speed, because there are no significant coronal holes in the input images in this case. We find that the reason for this enhancement originates from coronal mass ejections (CMEs). According to the Coordinated Data Analysis Web (CDAW) CME online catalog, a halo CME occurred at 2013 September 29, 22:12 UT with a speed of 1179 km s^{-1}. It arrived at the Earth at 2013 October 2 according to the Richardson–Cane ICME list (Richardson et al. 2000; Richardson & Cane 2010). This coincides with the time point at which the solar wind speed increases, so the ICME can be thought of as the reason for this. Our model cannot take the information about the CMEs from input data. To improve the performance of the model in this point, we try to modify the model with additional input data including CME information. We simply consider features of halo CMEs such as angular width, source regions, and speeds as input data with a 6 hr cadence. However, the performance of the model is not significantly different. We need to analyze the relationship between CMEs and solar wind speeds more deeply for a proper model design. We leave this work for a future study.

5. Summary

In this study, we make a solar wind speed prediction model up to 72 hr with 6 hr intervals using a deep-learning model. We use SDO/AIA 211 and 193 Å images and solar wind speeds themselves as input data for the model. The deep-learning model consists of two networks each for images and solar wind

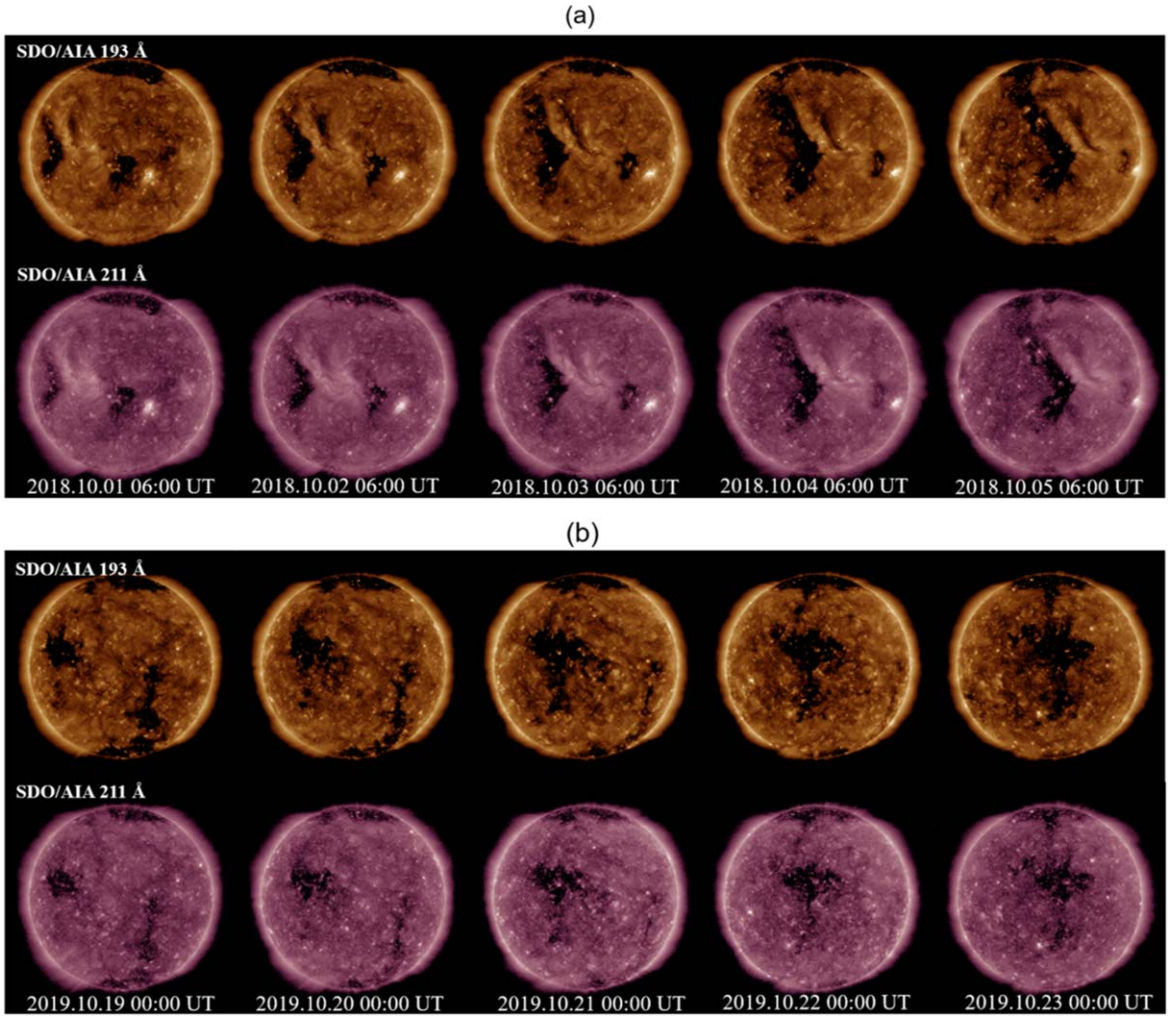

Figure 6. Panel (a) shows examples of input images for Figure 4(a), and panel (b) shows the same for Figure 4(b). Top images of each panel are 193 Å and bottom ones are 211 Å images. The equatorial coronal holes, the source of high-speed streams, are well shown in these input images.

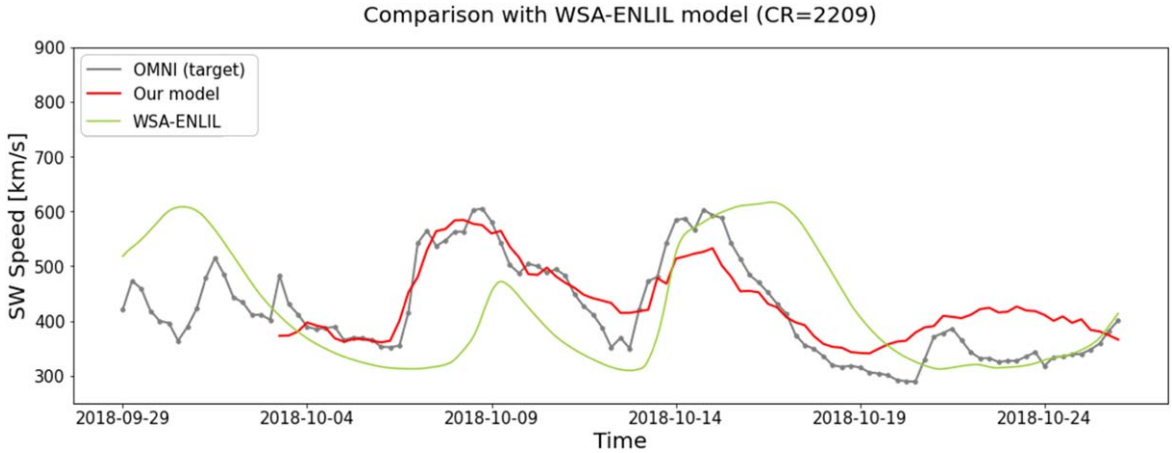

Figure 7. Comparison of the results of the 72 hr prediction by our model (red line) with those of the WSA-ENLIL model (green line) in CR 2209 where the period of Figure 4(a) is included. The gray line indicates the observed solar wind speeds.

data. The results of the study are as follows. The CC of our model is from 0.92 (for the 6 hr prediction) to 0.67 (for the 72 hr prediction), and the RMSE is from 37.4 to 68.2 km s^{-1}. These values are better than those of the previous models. The model successfully predicts solar wind speed increases such as corotating interaction regions, which are caused by equatorial coronal holes. The solar wind speed prediction results from our model are compared to those from the WSA-ENLIL model, and the results of our model show more consistency with near-Earth observations at CR 2209 than those of the WSA-ENLIL model. However, our model cannot predict solar wind speed enhancement caused by CMEs. For this, a deeper

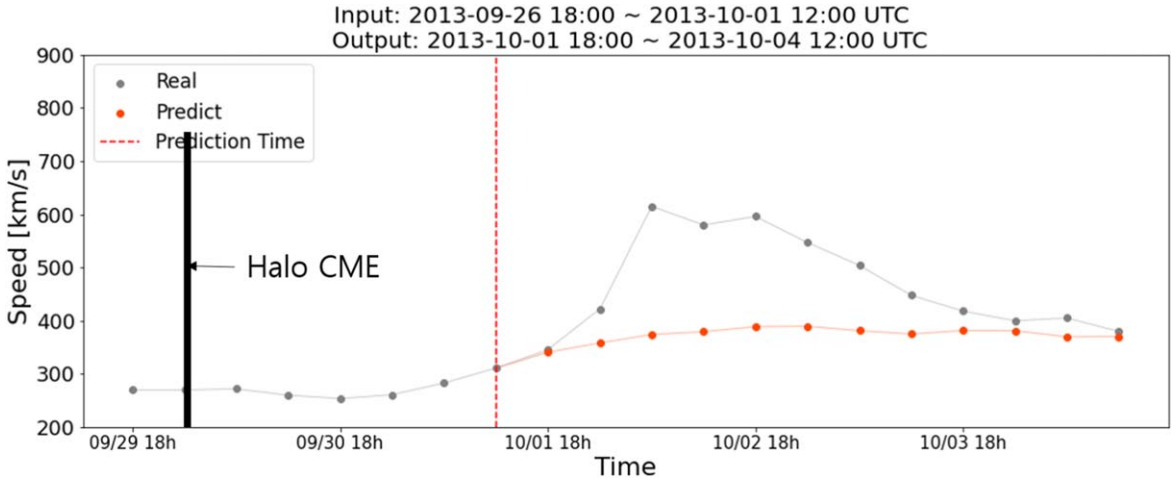

Figure 8. An example of poor prediction by our model. The gray line shows observation data, and the orange one shows prediction values by our model. The red dashed line is a forecast start time. The black solid line indicates a halo CME occurred at 2013 September 29.

understanding of the relationship between solar wind speed and CMEs will be needed. We leave this for a future work. We have proposed a deep-learning method using both image data and solar wind values in sequence simultaneously for the solar wind speed prediction, unlike the previous studies. Our model shows successful performance, which implies that our deep-learning method should be helpful for similar types of space weather forecasting.

Our study has a high potential for application in space weather forecasting. First, our study could be used for near-real-time forecasting. We think that there are two kinds of approaches for near-real-time applications. One approach is to make the data from OMNIWeb in near real time. The other approach is to make another deep-learning model using satellite observations directly, like from the Deep Space Climate Observatory. In addition, it is necessary to include how to handle missing or abnormal data. Our model also can be applied to the prediction at a point other than the Earth. It is possible with the same input data set if there are observational data of solar wind speeds at other stationary points (e.g., L5/L4 missions) with respect to the Earth. Including data from an L5 point (such as the Vigil mission) in our input data set may be helpful. Since coronal holes look different depending on the angle of view, the model will be able to get more detailed information on them.

Acknowledgments

This research was supported by Basic Science Research Program through the National Research Foundation of Korea (NRF) funded by the Ministry of Education (NRF-2021R1I1A1A01049615 and RS-2023-00248916), the Korea Astronomy and Space Science Institute under the R&D program (Project No. 2023-1-850-07) supervised by the Ministry of Science and ICT (MSIT), Institute of Information & Communications Technology Planning & Evaluation (IITP) grant funded by the Korean government (MSIT) (No. RS-2023-00234488, Development of solar synoptic magnetograms using deep learning), and National Meteorological Satellite Center (NMSC)/ Korea Meteorological Administration (KMA) (No. 33233031800). We acknowledge use of NASA/GSFC's Space Physics Data Facility's OMNIWeb (or CDAWeb or ftp) service, and OMNI data. We appreciate the GSFC/CCMC for providing a publicly available simulation service (https://ccmc.gsfc.nasa.gov). The CORHEL-MAS_WSA_ENLIL model was developed by the Jon Linker at Predictive Science. We acknowledge numerous team members who have contributed to the success of the SDO mission. We thank the community efforts devoted to developing of the open-source packages that were used in this work.

ORCID iDs

Jihyeon Son https://orcid.org/0000-0003-2678-5718
Yong-Jae Moon https://orcid.org/0000-0001-6216-6944
Harim Lee https://orcid.org/0000-0002-9300-8073
Hyun-Jin Jeong https://orcid.org/0000-0003-4616-947X

References

Altschuler, M. D., & Newkirk, G. 1969, SoPh, 9, 131
Arge, C. N., & Pizzo, V. J. 2000, JGR, 105, 10465
Bravo, S., & Stewart, G. A. 1997, ApJ, 489, 992
Bussy-Virat, C. D., & Ridley, A. J. 2014, SpWea, 12, 337
Choi, Y., Moon, Y. J., Choi, S., et al. 2009, SoPh, 254, 311
de Toma, G. 2011, SoPh, 274, 195
Elliott, H. A., Arge, C. N., Henney, C. J., et al. 2022, SpWea, 20, e2021SW002868
Gosling, J. T., & Pizzo, V. J. 1999, in Corotating Interaction Regions, ed. A. Balogh et al. (Dordrecht: Springer Netherlands), 21
Hassler, D. M., Dammasch, I. E., Lemaire, P., et al. 1999, Sci, 283, 810
Hochreiter, S., & Schmidhuber, J. 1997, Neural Comput., 9, 1735
Jian, L. K., MacNeice, P. J., Taktakishvili, A., et al. 2015, SpWea, 13, 316
King, J., & Papitashvili, N. 2005, JGRA, 110, A02104
Kingma, D. P., & Ba, J. 2014, arXiv:1412.6980
Klambauer, G., Unterthiner, T., Mayr, A., & Hochreiter, S. 2017, Advances in Neural Information Processing Systems 30, ed. I. Guyon et al. (Red Hook, NY: Curran Associates) https://papers.nips.cc/paper_files/paper/2017/hash/5d44ee6f2c3f71b73125876103c8f6c4-Abstract.html
Lemen, J. R., Title, A. M., Akin, D. J., et al. 2012, SoPh, 275, 17
Liu, D. D., Huang, C., Lu, J. Y., & Wang, J. S. 2011, MNRAS, 413, 2877
Nair, V., & Hinton, G. E. 2010, Proc. 27th Int. Conf. on Machine Learning (Madison, WI: Omnipress), 807, https://www.cs.toronto.edu/~fritz/absps/reluICML.pdf
Nolte, J. T., Krieger, A. S., Timothy, A. F., et al. 1976, SoPh, 46, 303
Odstrcil, D. 2003, AdSpR, 32, 497
Odstrcil, D., Mays, M. L., Hess, P., et al. 2020, ApJS, 246, 73
Owens, M. J., Challen, R., Methven, J., Henley, E., & Jackson, D. R. 2013, SpWea, 11, 225
Owens, M. J., Spence, H. E., McGregor, S., et al. 2008, SpWea, 6, S08001
Pesnell, W. D., Thompson, B. J., & Chamberlin, P. C. 2012, SoPh, 275, 3

Pitňa, A., Šafránková, J., Němeček, Z., Ďurovcová, T., & Kis, A. 2021, FrP, 8, 654
Poggi, P., Museli, M., Notton, G., Cristofari, C., & Louche, A. 2003, ECM, 44, 3177
Raju, H., & Das, S. 2021, SoPh, 296, 134
Reiss, M. A., MacNeice, P. J., Muglach, K., et al. 2020, ApJ, 891, 165
Richardson, I. G., & Cane, H. V. 2010, SoPh, 264, 189
Richardson, I. G., Cliver, E. W., & Cane, H. V. 2000, JGR, 105, 18203
Rotter, T., Veronig, A., Temmer, M., & Vršnak, B. 2015, SoPh, 290, 1355
Sachdeva, N., van der Holst, B., Manchester, W. B., et al. 2019, ApJ, 887, 83
Schatten, K. H. 1971, CosEl, 2, 232
Schatten, K. H., Wilcox, J. M., & Ness, N. F. 1969, SoPh, 6, 442
Sun, Y., Xie, Z., Chen, Y., Huang, X., & Hu, Q. 2021, SpWea, 19, e2020SW002707
Szegedy, C., Liu, W., Jia, Y., et al. 2014, arXiv:1409.4842
Tsurutani, B. T., Gonzalez, W. D., Gonzalez, A. L. C., et al. 2006, JGRA, 111, A07S01
Upendran, V., Cheung, M. C., Hanasoge, S., & Krishnamurthi, G. 2020, SpWea, 18, e2020SW002478
Vršnak, B., Temmer, M., & Veronig, A. M. 2007a, SoPh, 240, 315
Vršnak, B., Temmer, M., & Veronig, A. M. 2007b, SoPh, 240, 331
Wang, Y. M., & Sheeley, N. R. J. 1990, ApJ, 355, 726
Wang, Y. M., & Sheeley, N. R. J. 1992, ApJ, 392, 310
Yang, Y., Shen, F., Yang, Z., & Feng, X. 2018, SpWea, 16, 1227
Zirker, J. B. 1977, RvGSP, 15, 257